

## Article

# Impact of Rejuvenator-Modified Mastic on Asphalt Mixture Stiffness: Meso-Scale Discrete Element Method Approach

Gustavo Câmara <sup>1,\*</sup> , Nuno Monteiro Azevedo <sup>2</sup>  and Rui Micaelo <sup>3</sup> 

<sup>1</sup> Department of Civil Engineering, School of Science and Technology, Universidade NOVA de Lisboa, 2829-516 Caparica, Portugal

<sup>2</sup> Concrete Dams Department, National Laboratory for Civil Engineering, 1700-111 Lisbon, Portugal; nazevedo@lnec.pt

<sup>3</sup> CERIS, Department of Civil Engineering, School of Science and Technology, Universidade NOVA de Lisboa, 2829-516 Caparica, Portugal; ruilbm@fct.unl.pt

\* Correspondence: g.camara@campus.fct.unl.pt

**Abstract:** Encapsulated rejuvenators embedded in asphalt mixtures are a promising technology to extend the service life of asphalt pavements. However, their effects on the asphalt mixture's performance still need to be properly understood. A recently developed three-dimensional discrete element method framework enables the evaluation of non-homogeneous distributions of the rejuvenator, closely resembling real conditions. This includes different scenarios involving capsule content and release efficiency. The presented numerical results show that the rejuvenator-to-mastic ratio and the number of rejuvenator-modified contacts influence the stiffness properties of asphalt mixtures. In cases where a homogeneous rejuvenator distribution is assumed, the three-dimensional DEM model predicts a significant reduction in the asphalt mixture's stiffness that compromises the pavement's performance. Simulations show that the diffusion effect needs to be considered for predicting the post-healed behavior of asphalt mixtures. For cases considering more suitable modified mastic amounts (less than 1.20 wt%), the effect on the asphalt mixture's stiffness modulus is less pronounced, and the phase angle is not significantly affected. Additionally, the presented simulations suggest that the capsule content can be increased up to 0.75 wt%, and capsules with a release rate higher than 48% can be used without compromising the rheological performance of asphalt mixtures, possibly improving their self-healing properties. These numerical insights should be considered in future designs to achieve optimal post-healed behavior.

**Keywords:** discrete element modeling; self-healing; asphalt mixture; rejuvenator-modified mastic; encapsulated rejuvenator; capsules



**Citation:** Câmara, G.; Azevedo, N.M.; Micaelo, R. Impact of Rejuvenator-Modified Mastic on Asphalt Mixture Stiffness: Meso-Scale Discrete Element Method Approach. *Buildings* **2023**, *13*, 3023. <https://doi.org/10.3390/buildings13123023>

Academic Editor: Pengfei Liu

Received: 13 November 2023

Revised: 30 November 2023

Accepted: 3 December 2023

Published: 5 December 2023



**Copyright:** © 2023 by the authors. Licensee MDPI, Basel, Switzerland. This article is an open access article distributed under the terms and conditions of the Creative Commons Attribution (CC BY) license (<https://creativecommons.org/licenses/by/4.0/>).

## 1. Introduction

Asphalt mixtures are the most common road surfacing material [1], usually adopted due to their positive performance under traffic loading, low surface friction resistance, low traffic noise, and sustainability aspects [2,3]. The expected service life of asphalt pavements ranges between fifteen to thirty years [4]. However, these structures are prone to damage due to temperature changes, UV radiation, aging, moisture damage, and repeated traffic loads, progressively reducing their lifespan [5,6]. This detrimentally impacts users' comfort and safety conditions, leading to increased maintenance operations, which may result in environmental impacts [7] and expenses. Damage occurs regardless of the asphalt mixture's endogenous self-healing capacity [8], which implies that microcracks are autonomously closed due to the flow capacity of the asphalt binder. Still, the self-healing process, influenced by in-service temperature conditions and continuous traffic [1], may take several days. Consequently, the damage rate surpasses the healing rate, allowing microcracks to propagate and increase in size. Over the past decade, researchers have explored several methods to overcome these limitations, including induction heating [9],

microwave heating [10], encapsulated rejuvenators [11], and combined methodologies [12]. These methods aim to improve the healing rate, extend the pavement service life, and reduce the frequency and costs of maintenance operations. A recent study has shown that these approaches may contribute to a 30% reduction in energy consumption and CO<sub>2</sub> emissions during the life cycle [13]. Compared with other technologies, the encapsulated rejuvenator-based healing method has the additional advantage of not requiring further intervention to trigger healing mechanisms.

Rejuvenators have been recognized for improving the healing properties and durability of asphalt mixtures [14] and regenerating the aged asphalt binder [15]. The influence of capsules on the mechanical properties of asphalt mixtures, e.g., the stiffness modulus, may impact the design of asphalt pavement thickness layers [16]. For instance, Micaelo et al. [17] indicated that calcium-alginate capsules may negatively affect the deformation resistance of mixtures because of the released rejuvenator during their fabrication. García et al. [18] showed that specimens with capsules have a lower stiffness (indirect tensile tests) compared to samples without, possibly due to the capsule's lower mechanical strength. Al-Mansoori et al. [1] reported similar results, although the water sensitivity, particle loss, and permanent deformation between mixtures with and without capsules were alike. The authors, however, attributed the lower stiffness to the large capsule size. Despite the possible negative impacts on the stiffness of mixtures, the incorporation of capsules has been reported as positive for improving the self-healing properties without significantly compromising other mechanical characteristics. Norambuena-Contreras et al. [8] suggested that these healing elements improve the mechanical and healing properties of asphalt materials. However, higher capsule contents (0.75 and 1.00 wt%) might reduce the average fatigue life. Norambuena-Contreras et al. [5] registered similar differences in the modulus and other mechanical properties of mixtures, e.g., tensile strength, fatigue resistance, and water sensitivity, containing the same amount of capsules. Besides the slight impact on the stiffness properties of mixtures, possibly because the adopted capsules are highly deformable and softer than aggregates, Micaelo et al. [19] suggested that capsules enhance their rutting resistance. Kargari et al. [20] verified analogous effects by adopting a hybrid system (encapsulated method and microwave heating).

The released rejuvenator has a direct impact on the asphalt binder in the surrounding area of the capsule location. The rheological and healing properties of this binder undergo significant changes, influenced by factors such as the type of rejuvenator and the amount released in the specified zone [21]. In their comprehensive study, Xu et al. [22] investigated three distinct rejuvenators, classifying each based on its efficiency in softening the aged bitumen to the required level with minimal amounts. Wang et al. [23] assessed the impact of rejuvenators on the rheological properties and diffusion rates of asphalt binders, confirming their capacity to restore the viscosity of aged binders. Other investigations have reported similar results with different rejuvenator types, considering environmental perspectives. For instance, Li et al. [24] verified a similar reduction in the binder viscosity using bio-oil. Additionally, Norambuena-Contreras et al. [25] demonstrated how waste cooking oil, specifically recycled sunflower oil, can permeate aged bitumen, reducing its viscosity and thereby enhancing its self-healing capabilities. Regardless of the significant benefits highlighted in experimental studies, the encapsulated rejuvenator effect in asphalt mixtures still requires further elucidation.

The discrete element method (DEM), initially devised for granular materials [26] and introduced for asphalt materials in the 1990s, has been extensively adopted by pavement researchers [27–29]. Compared to the finite element method, the DEM offers several advantages: (1) it directly considers the material grain structure, including its randomness, (2) it can be adopted in the model generation, (3) for the same level of refinement, the DEM requires less computational resources, and (4) fracture is straightforward due to its discrete nature. Thus, the DEM provides a framework to further evaluate the rejuvenator effect on the asphalt mixture's macroscopic properties. Most numerical DEM models were initially developed in two dimensions and adopted elastic models to describe the

behavior of asphalt materials due to lower computational costs. Abbas et al. [30], utilizing the DEM, investigated the rheological behavior of asphalt materials under dynamic tests, revealing that numerical results underpredicted the modulus in most simulations. With the increasing computational efficiency over the years, three-dimensional (3D) models and the implementation of more complex contact models have become more accessible. Al Khateeb et al. [31] modeled the compaction process of mixtures and confirmed that temperature drop adversely affects compaction, possibly associated with an increased viscous state degree of the mastic (bitumen and fine aggregates) at lower temperatures. In a similar study, Liu et al. [32] assessed the impact of the paving speed on the compaction process of asphalt pavements. Meanwhile, Peng et al. [33] demonstrated that the number of repeated loads, temperature, and crumb rubber content are influential parameters for the permanent deformation of asphalt pavements. Recently, numerical models have been developed to study the micro-mechanics of the healing effects on asphalt mixtures. Zhang et al. [34] assessed the self-healing capacity by adopting two healing models, verifying that the gradual increase in accumulated damage reduces the healing ratio of mixtures. Câmara et al. [35] evaluated the influence of sunflower oil (rejuvenator) on the shear stiffness properties of mastics, highlighting the benefits of incorporating complex contact models in numerical simulations.

## 2. Objectives and Scope

The recently developed 3D DEM VirtualPASM3D Lab framework has been successfully applied in predicting the behavior of asphalt mixtures given a previous calibration of the particles representing the mastic, using known experimental results, and considering the aggregate Young's modulus [36]. This modeling approach considers the asphalt mixture as a heterogeneous material, where part of its mastic phase holds more pronounced deformable properties. In a recent work, the mastic contact properties with different oil contents were defined using dynamic shear rheometer (DSR) tests [35].

In the present work, both studies have been combined, allowing the assessment of the influence of rejuvenator-modified mastic particles, also referred to as activated capsules, on the stiffness properties of asphalt mixtures under uniaxial tension–compression dynamic tests. These rejuvenator-modified mastic particles represent the blend between the mastic and the rejuvenator.

This numerical investigation focuses on modeling the post-healed state of the asphalt mixture, which has been damaged and healed by the effect of the rejuvenator released from embedded capsules and does not intend to represent the actual capsules. Different contact parameters define the randomly selected rejuvenator-modified mastic particles within the mastic phase, allocating the rejuvenator effect based on previous experimental results.

The presented numerical simulations aim to contribute to the assessment of factors that may influence the behavior of asphalt mixtures. This includes a focus on the non-homogeneous distributions of the rejuvenator, the rejuvenator-to-mastic ratio based on the rejuvenator release rate from capsules, the number of modified mastic particles, and the volume of influence assigned to the capsules to effectively manage the rejuvenator's efficiency within the particle assembly.

The adopted 3D DEM framework is initially described, followed by the presentation of the asphalt mixture particle model. Then, the numerical simulations to assess the effect of the encapsulated rejuvenator are presented and the predicted results are discussed.

## 3. 3D DEM Adopted Framework

The VirtualPASM3D Lab program adopted in this study has proven to be a valid approach for modeling and predicting the behavior of asphalt mastics and asphalt mixtures [36]. The adopted DEM model directly represents aggregates and mastic particles. In contrast to alternative DEM approaches that employ a more detailed discretization of the internal composition of asphalt mixtures, the present approach operates with a reduced computational cost. As shown in [36], time-dependent contact models improve simula-

tion results by representing the aggregate-to-mastic and mastic-to-mastic interactions that generally exist in asphalt mixtures, rather than adopting elastic contact models. Therefore, this numerical study adopted a generalized Kelvin (GK) contact model, which has been previously validated for mastics and asphalt mixtures [36].

### 3.1. Generalized Kelvin Contact Model Formulation

The generalized Kelvin contact model comprises a Maxwell model unit, which corresponds to elastic spring ( $\kappa_m$ ) and visco-plastic dashpot ( $\eta_m$ ) portions, and  $j$ -Kelvin elements, represented by springs ( $\kappa_{[1-j]}$ ) and dashpots ( $\eta_{[1-j]}$ ) connected in parallel, that correspond to the delayed elastic portion of the model. These components are placed in series, as illustrated in Figure 1.

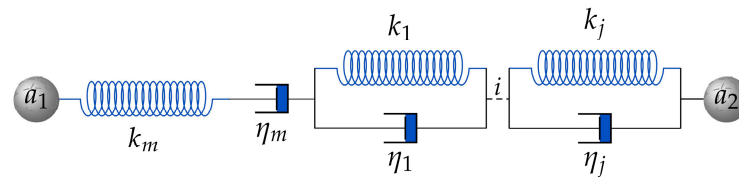


**Figure 1.** Generalized Kelvin contact model representation.

Based on the fact that the elements of the contact model are placed in series, the equations regarding the contact model total displacement ( $u$ ) and the resulting contact model force ( $f$ ) are expressed by:

$$u = u_{el} + u_{vp} + \sum_{i=1}^j u_{ve}^i \quad (1)$$

$$f = f_{el} = f_{vp} = f_{ve}^i$$

where  $u_{el}$ ,  $u_{vp}$ , and  $u_{ve}^i$  are the displacement for the elastic, visco-plastic, and delayed elastic portions, while  $f_{el}$ ,  $f_{vp}$ , and  $f_{ve}^i$  are their respective contact forces.

The GK contact model derives from the direct integration using a time-centered difference scheme for the force and displacement relationships. Therefore, the displacement expressions for the elastic, visco-plastic, and delayed elastic elements are given by:

$$u_{el} = \frac{f}{\kappa_m} \quad (2)$$

$$\dot{u}_{vp} = \frac{f}{\eta_m} \quad (3)$$

$$\dot{u}_{ve}^i = \frac{f - \kappa_i u_{ve}^i}{\eta_i} \quad (4)$$

The displacement of the  $i$ -th element from the delayed elastic portion at time  $t + \Delta t$  is determined based on Equation (4) by applying the time-centered difference approximation for the derivative elements and average values for the force,  $f$ , and displacement,  $u_{ve}^i$ , as expressed by:

$$u_{ve}^{i, t+\Delta t} = \frac{1}{A_i} \left[ u_{ve}^{i, t} B_i + \frac{\Delta t (f^{t+\Delta t} + f^t)}{2\eta_i} \right] \quad (5)$$

where  $\Delta t$  is the time step,  $f^{t+\Delta t}$  and  $f^t$  are the contact forces of the model at times  $\Delta t$  and the previous step, and  $u_{ve}^{i, t}$  is the viscoelastic displacement at the prior step. The components  $A_i$  and  $B_i$  are given by:

$$A_i = 1 + \frac{\kappa_i \Delta t}{2\eta_i} \quad (6)$$

$$B_i = 1 - \frac{\kappa_i \Delta t}{2\eta_i}$$

The first derivative for the displacement corresponding to the Maxwell model (elastic and visco-plastic portions) as part of the GK contact model is described as follows:

$$\dot{u}_m = \dot{u}_{el} + \dot{u}_{vp} \quad (7)$$

After calculating and substituting the first derivative of Equations (2) and (3), Equation (7) becomes:

$$\dot{u}_m = \frac{\dot{f}}{\kappa_m} + \frac{f}{\eta_m} \quad (8)$$

Similar to the Kelvin portion of the GK contact model, the displacement corresponding to the Maxwell unit (elastic and visco-plastic components) at time  $t + \Delta t$  is determined based on Equation (8) by applying the time-centered difference approximation for the derivative elements and the average value for the force,  $f$ , as given by:

$$u_m^{t+\Delta t} = \frac{f^{t+\Delta t} - f^t}{\kappa_m} + \frac{\Delta t (f^{t+\Delta t} + f^t)}{2\eta_m} + u_m^t \quad (9)$$

The total contact force of the GK contact model is determined after calculating the first derivative for the total displacement (Equation (1)), applying the time-centered approximation for the time derivatives, and substituting Equations (5) and (9), as follows:

$$f^{t+\Delta t} = \frac{1}{C} \left[ u^{t+\Delta t} - u^t + \sum_{i=1}^j \left( u_{ve}^{i,t} - \frac{B_i u_{ve}^{i,t}}{A_i} \right) - D f^t \right] \quad (10)$$

where the components  $C$  and  $D$  are calculated accordingly:

$$C = \sum_{i=1}^j \left( \frac{\Delta t}{2A_i \eta_i} \right) + \frac{1}{\kappa_m} + \frac{\Delta t}{2\eta_m} \quad (11)$$

$$D = \sum_{i=1}^j \left( \frac{\Delta t}{2A_i \eta_i} \right) - \frac{1}{\kappa_m} + \frac{\Delta t}{2\eta_m}$$

### 3.2. Calibration of Contact Model Parameters

Contact models are microscale mechanical models that define the interactions between particles or two elements based on known parameters. As previously mentioned, experimental results describe the macroscopic behavior of the material. Consequently, the parameters associated with contact models, reflecting the micromechanical properties of the material, are often challenging to derive from laboratory tests and need to be initially estimated. In order to calculate the GK contact model parameters, a macroscopic generalized Kelvin model (Figure 2), defining material properties, was first established to fit laboratory test results, particularly the dynamic modulus and phase angle of asphalt binders obtained from sinusoidal loading tests. This fitting procedure is typically more difficult for generalized models due to the higher number of unknown variables and thus requires more steps. The advantage of this method lies in defining a single set of contact parameters across all test frequencies for each asphalt material.

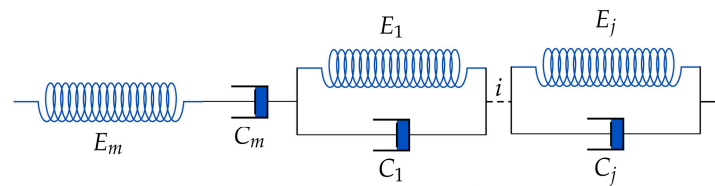


**Figure 2.** Macroscopic generalized Kelvin model representation.

In Figure 2,  $E_m$  and  $C_m$  are the elastic and visco-plastic portions of the Maxwell unit, and  $E_{[1-j]}$  and  $C_{[1-j]}$  correspond to the elements composing the delayed elastic of the macroscale model, where  $j$  is the number of Kelvin units.

The fitting process is based on minimizing an objective function ( $F$ ), which relates the analytically predicted values, and the laboratory test results for the real and imaginary portions of the dynamic modulus (norm of the complex modulus) across the available range of testing frequencies. The calculation process to predict the analytical values for the dynamic modulus and phase angle to further define the macroscale properties and the number of Kelvin units for the GK contact model is described in [36]. The objective function is given by:

$$F = \sum_{z=1}^n \left[ \left( \frac{E'_z}{E_z'^0} - 1 \right)^2 + \left( \frac{E''_z}{E_z''^0} - 1 \right)^2 \right] \quad (12)$$

where  $E'_z$  and  $E''_z$  are the real and imaginary components of the complex modulus predicted at the  $z$ -th frequency,  $E_z'^0$  and  $E_z''^0$  are the laboratory values of the real and imaginary components of the complex modulus measured at the  $z$ -th frequency, and  $n$  is the number of data points. In the complex plane, the real and imaginary components of the complex modulus correspond to the storage modulus and the loss modulus, respectively.

The mastic contact properties were adopted following the calibration presented by Câmara et al. [35]. In their study, Câmara et al. analyzed the effect of different rejuvenator-to-bitumen ratios (2.5%, 5%, 10%, and 20%, by weight of bitumen) on the stiffness properties of mastics, thereby validating the laboratory results with a DEM mastic model. For each mastic specimen, distinct contact parameters characterize the rejuvenator content mixed in the asphalt mastic.

In the present study, asphalt mixtures incorporate rejuvenator-modified mastic particles representing the blend between the mastic and the sunflower oil released from capsules. Virtual asphalt mixtures may have interactions involving rejuvenator-modified mastic particles and other contacts related to mastic elements that remain original. Therefore, two types of time-dependent contact properties are defined: non-modified and rejuvenator-modified contacts.

The viscoelastic contact parameters define the influence of the rejuvenator on the mastic, varying with several rejuvenator-modified mastic particle ratios. These ratios are based on the rejuvenator-to-bitumen ratio [35], emulating the volume of healing agent released from capsules in the numerical model. The contact properties representing the rejuvenator content in the modified mastic particles are denoted as CM-2.5, CM-5, CM-10, and CM-20 (CM—contact modified), which express the influence of the 2.5%, 5%, 10%, and 20% rejuvenator-to-bitumen ratios, respectively, in the particle assembly. Interactions involving mastic particles without the presence of a rejuvenator are referred to as CM-0.

Table 1 shows the macroscale properties of both non-modified and rejuvenator-modified asphalt mastics that define the different interactions within the mixture. In this study, a minimum of seven Kelvin units was found to adequately capture the time-dependent behavior of the asphalt binder and achieve minimal error. The macroscale parameters and the number of Kelvin units indirectly describe the influence of the rejuvenator content on the asphalt mastic.

**Table 1.** Macroscale properties of non-modified and rejuvenator-modified mastics.

Property Type	CM-0		CM-2.5		CM-5		CM-10		CM-20	
Chains	$E_i$ (kPa) <sup>a</sup>	$C_i$ (kPa·s) <sup>b</sup>	$E_i$	$C_i$	$E_i$	$C_i$	$E_i$	$C_i$	$E_i$	$C_i$
1	$2.3 \times 10^5$	$2.3 \times 10^2$	$1.3 \times 10^5$	$1.3 \times 10^2$	$7.3 \times 10^4$	$7.3 \times 10^1$	$3.1 \times 10^4$	$3.1 \times 10^1$	$5.2 \times 10^2$	$5.2 \times 10^0$
2	$1.2 \times 10^5$	$1.2 \times 10^3$	$6.2 \times 10^4$	$6.2 \times 10^2$	$3.5 \times 10^4$	$3.5 \times 10^2$	$1.1 \times 10^4$	$1.1 \times 10^2$	$2.3 \times 10^2$	$2.3 \times 10^1$
3	$2.7 \times 10^4$	$2.7 \times 10^3$	$1.1 \times 10^4$	$1.1 \times 10^3$	$6.2 \times 10^3$	$6.2 \times 10^2$	$2.0 \times 10^3$	$2.0 \times 10^2$	$6.3 \times 10^1$	$6.3 \times 10^1$
4	$5.9 \times 10^3$	$5.9 \times 10^3$	$2.5 \times 10^3$	$2.5 \times 10^3$	$1.3 \times 10^3$	$1.3 \times 10^3$	$4.5 \times 10^2$	$4.5 \times 10^2$	$1.8 \times 10^1$	$1.8 \times 10^2$
5	$1.3 \times 10^3$	$1.3 \times 10^4$	$5.9 \times 10^2$	$5.9 \times 10^3$	$3.9 \times 10^2$	$3.9 \times 10^3$	$1.6 \times 10^2$	$1.6 \times 10^3$	$2.9 \times 10^{-1}$	$2.9 \times 10^1$
6	$3.5 \times 10^2$	$3.5 \times 10^4$	$2.3 \times 10^2$	$2.3 \times 10^4$	$1.4 \times 10^2$	$1.4 \times 10^4$	$8.1 \times 10^1$	$8.1 \times 10^3$	$4.7 \times 10^2$	$4.7 \times 10^5$
7	$1.9 \times 10^2$	$1.9 \times 10^5$	$1.7 \times 10^1$	$1.7 \times 10^4$	$4.6 \times 10^4$	$4.6 \times 10^7$	$2.4 \times 10^0$	$2.4 \times 10^3$	$5.3 \times 10^2$	$5.3 \times 10^6$
8	$5.2 \times 10^0$	$5.2 \times 10^4$	$7.4 \times 10^{-1}$	$7.4 \times 10^3$	$4.3 \times 10^{-1}$	$4.3 \times 10^3$	$4.7 \times 10^{-2}$	$4.7 \times 10^2$	-	-
9	$4.5 \times 10^3$	$4.5 \times 10^8$	-	-	-	-	-	-	-	-
$E_m$	$3.4 \times 10^5$		$2.8 \times 10^5$		$3.8 \times 10^5$		$2.8 \times 10^5$		$2.9 \times 10^3$	
$C_m$	$3.0 \times 10^3$		$9.0 \times 10^2$		$3.6 \times 10^2$		$7.7 \times 10^1$		$3.0 \times 10^0$	

<sup>a</sup> This unit applies to any  $E_i$  and  $E_m$ , regardless of the contact property type. <sup>b</sup> This unit applies to any  $C_i$  and  $C_m$ , regardless of the contact property type.

In the next step, the lab-based macroscale material properties were converted into contact parameters for assignment in the DEM simulations. In this case, a viscoelastic beam, described by two contacting particles with its ends at the centers of the two elements, was employed to represent mastic properties. This process adopts the strain and stress relationships derived from the viscoelastic beam to compute the contact parameters of the GK contact model for the normal direction. Upon obtaining the macroscale properties, the contact parameters are derived from the following expression:

$$\kappa_{\zeta}^n = \frac{E_{\zeta} A}{L} \delta \quad (13)$$

$$\eta_{\zeta}^n = \frac{C_{\zeta} A}{L} \delta$$

where  $A$  is the contact area of the particles,  $L$  is the summation of the two particles' radii,  $\delta$  is a coefficient to adjust possible differences between the macroscopic properties and the DEM parameters, and  $\zeta$  indicates  $i$  for the  $i$ -th element of the viscoelastic portion and  $m$  for the Maxwell element (elastic and visco-plastic components) of the GK contact model.

Furthermore, the contact parameters corresponding to the tangent direction are calculated based on the product of the contact stiffness ratio,  $\alpha$  ( $\kappa_s/\kappa_n$ ), and the estimated values for the normal direction. The coefficient of adjustment that relates micro–macro-properties and the contact stiffness ratio for the time-dependent contacts were 1.88 and 0.10, respectively. These values have been identified as the coefficients that provide the most accurate prediction of the asphalt mixture's behavior [36].

#### 4. Numerical Modeling of Asphalt Mixture Affected by the Encapsulated Rejuvenators

##### 4.1. Particle Generation Procedure of Standard Asphalt Mixture

A virtual specimen of the asphalt mixture (AM), with rigid spherical particles, was created by adopting a random generation method. The method, which is easier to implement with respect to image-based methods, is laboratory non-dependent and can represent the heterogeneity of asphalt mixtures. The asphalt mixture is considered to be composed of coarse aggregates (size larger than 2.0 mm) and mastic (a combination of aggregates smaller than 2.0 mm and bitumen). The aggregate phase was initially inserted in the defined space, computing the particles from the highest to the smallest diameters. The remaining void space was filled with mastic particles (smaller particles), represented by spherical elements with diameters ranging from 1.5 to 2.0 mm. Additional details regarding the adopted particle generation procedure are available in [36].

A prismatic numerical sample with dimensions of  $80 \times 50 \times 50$  mm<sup>3</sup>, containing 27,646 particles and 160,252 contacts, was generated to represent the asphalt mixture in

numerical simulations. This virtual specimen was created according to the aggregate gradation based on a previous asphalt mixture numerical study [36]. Table 2 shows the number of aggregate and mastic particles corresponding to the particles retained on each sieve size, along with their equivalent volumetric characteristics within the virtual specimen.

**Table 2.** Aggregate gradation and numerical particle representatives.

Sieve size (mm)	Aggregates					Mastic
	19	12.5	9.5	4.75	2	>2
Particles	-	13	29	309	2388	24,907
Volume (mm <sup>3</sup> )	-	27,794.5	20,957.6	39,365.8	25,788.0	64,830.3

The reference asphalt mixture comprises two material phases, including the aggregates and asphalt mastic. Additionally, the walls are structures where the loading conditions are applied. Hence, five different contact types exist in the numerical sample, corresponding to the aggregate-to-aggregate, aggregate-to-wall, mastic-to-wall, mastic-to-mastic, and the interface aggregate-to-mastic. The elastic and GK contact models were implemented to represent the existing contacts.

The elastic contact model characterizes the interactions within the aggregate phase and those involving the walls with any other particle. The GK contact model describes the behavior within the mastic phase and the aggregate-to-mastic contacts. Figure 3 illustrates the asphalt mixture (reference sample) and its two composing material phases. In Figure 3a, different colors are assigned to represent the aggregate particles retained on each sieve size. For the asphalt mixture's numerical representation (Figure 3c), the aggregate portion is uniformly depicted in one color to enhance the clarity of the particle model.

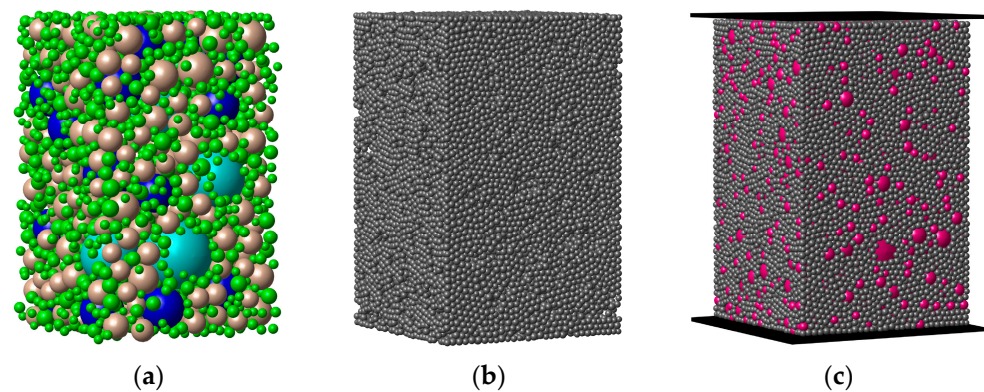


**Figure 3.** Particle model generation of standard asphalt mixture: (a) aggregate phase, (b) mastic phase, and (c) asphalt mixture.

The aggregate phase is considered to be elastic. Monotonic compression numerical tests were adopted to calibrate its elastic parameters. After proper calibration, the elastic modulus of aggregates ( $E_a$ ) was 61 GPa, the Poisson ratio was 0.26, and the contact stiffness ratio was 0.05. Additionally, the stiffness,  $\kappa_a$ , defining the elastic contact representation in the DEM simulations is given by:

$$\kappa_a = 2E_a \quad (14)$$

The macroscopic properties defining the time-dependent contact model are outlined in Table 1 and converted into contact parameters using Equation (13). The contact parameters for the aggregate-to-mastic interactions were determined after placing the generalized Kelvin contact model (asphalt mastic) and the elastic contact model (aggregate) in series,

where an equivalent stiffness ( $\kappa_{eq}$ ) was computed to replace  $\kappa_m$  of the elastic portion of the GK contact model. The equivalent stiffness results from the following calculation:

$$\kappa_{eq} = \frac{\kappa_a \kappa_m}{\kappa_a + \kappa_m} \quad (15)$$

#### 4.2. Numerical Model of the Effect of Encapsulated Rejuvenators

The numerical model introduces activated capsules modeled as rejuvenator-modified mastic particles dispersed in the mastic phase, i.e., it models the effect of the released rejuvenator on the mastic located in the volume where the capsules are located. To this end, mastic particles were randomly selected and converted to rejuvenator-modified ones based on the capsule amount adopted in the numerical simulation. These modified mastic particles emulate the effect that the rejuvenator released from embedded capsules has on the original mastic. The modified mastic particles had diameter sizes varying from 1.5 and 2.0 mm, with an average value of about 1.7 mm. Experimental analyses have tested capsules with similar dimensions, which may slightly differ depending on their morphology and structure [7,37,38].

This study considered the results and material properties reported in [35], in which the densities of bitumen, filler (fine aggregates), and asphalt mastic were 1.03 g/cm<sup>3</sup>, 2.71 g/cm<sup>3</sup>, and 1.64 g/cm<sup>3</sup>, respectively. The density, smoke point, and flash point of the commercial sunflower oil were 0.92 g/cm<sup>3</sup>, 227 °C, and 316 °C, respectively. In addition, the relationships between the volumes of the rejuvenator and asphalt mastic described by the contact properties CM-2.5, CM-5, CM-10, and CM-20 were 1.7%, 3.4%, 6.6%, and 12.4%, respectively.

#### 4.3. Study Cases

Different analyses were carried out to assess the impact of rejuvenator-modified mastic particles on the rheological properties of asphalt mixtures. In addition to the two material phases (aggregate and asphalt mastic) in the reference numerical specimen (Figure 3), the self-healing asphalt mixture in this study includes rejuvenator-modified particles that interact with aggregate and mastic elements. These contacts adopted the GK contact model with modified contact parameters (see Table 1).

The percentages of modified mastic particles adopted in the simulations represent the effect of broken capsules (activated) on the surrounding mastic. Experimental reports have shown that approximately 50% to 65% of capsules release rejuvenator [4,39], depending on the capsule properties and loading conditions.

To achieve the experimental volume ratios of rejuvenator/mastic (1.7%, 3.4%, 6.6%, and 12.4%) [35], the rejuvenator release rate ( $R$ ) from capsules is given by:

$$R(\%) = \frac{VR_{o/m} V_{oil-influence}}{V_{oil/caps}} \quad (16)$$

where  $VR_{o/m}$  is the volume ratio of rejuvenator/mastic from experimental analysis,  $V_{oil-influence}$  is the volume affected by the rejuvenator, and  $V_{oil/caps}$  is the rejuvenator volume in the capsule. From experimental-based investigations with calcium-alginate capsules [37,39,40], the encapsulated rejuvenator corresponded to approximately 62% of the capsule volume. Considering a capsule with an average modified-mastic diameter size (1.7 mm) in the numerical model, the value of  $V_{oil/caps}$  was 1.57 mm<sup>3</sup>.

This study assesses the influence of rejuvenator-modified mastic elements over two distinct aspects: (i) the effect of the rejuvenator amount dissolved in the modified mastic and (ii) the effect of the modified mastic particle content. The modified mastic particle content varies with the content of capsules in the mixture and the volume around broken capsules affected by the released rejuvenator. Three cases were studied in this context and detailed in the following subsections.

#### 4.3.1. Case 1

This case defines a baseline model representing the lower limit of the rheological behavior of the asphalt mixture. In this numerical model, the entire set of asphalt mastic particles was converted into rejuvenator-modified mastic elements. Accordingly, all particle interactions within the virtual specimen involving any of these components, which include aggregate-to-mastic, mastic-to-mastic, and mastic-to-wall contacts, were affected. As a result, these interactions are considered to receive rejuvenator-modified contact properties. Figure 4 illustrates the numerical sample for Case 1.

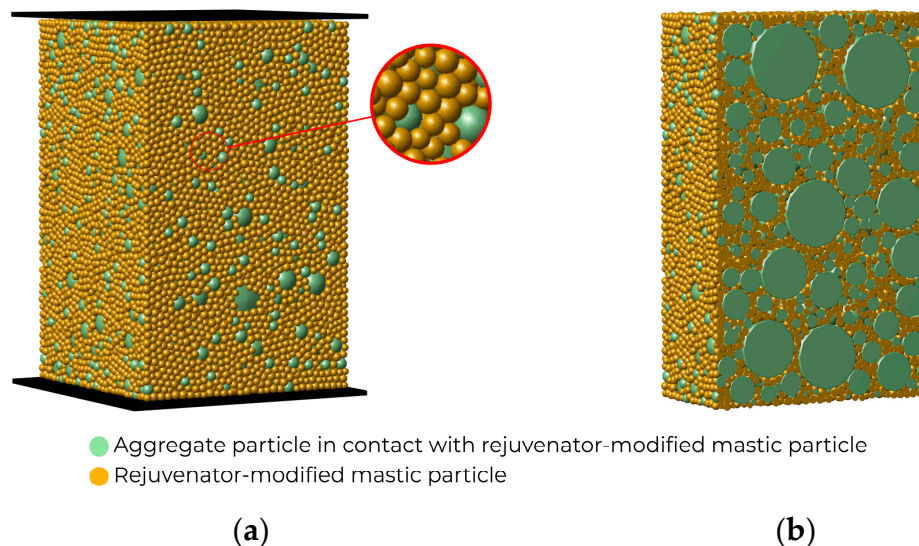


**Figure 4.** Asphalt mixture with mastic phase as rejuvenator-modified particles (case 1): (a) numerical sample and (b) cross-section at mid-point.

#### 4.3.2. Case 2

The preceding case (Case 1) illustrated a hypothetical scenario. In actual conditions, modifying the entire binder portion is not feasible because capsules are randomly dispersed and exert limited influence in asphalt mixtures. Therefore, simulations involving asphalt mixtures should also be conducted with a more realistic number of activated capsules.

In Case 2, a capsule content of 0.30 wt% (by weight of asphalt mixture) was utilized, with each capsule modifying the mastic particle located at its position and its neighboring contacts. Consequently, the volume of influence was limited to the capsule size (average diameter: 1.7 mm). This specific case represents an upper-limit model, where capsules containing the rejuvenator have a reduced rejuvenator volume effect. In this instance, 235 mastic particles were converted into rejuvenator-modified elements, thereby modifying 2326 contacts with appropriately assigned contact parameters.

The 0.30 wt% ratio has been attributed as a reasonable value for promoting the self-healing and mechanical properties of asphalt mixtures based on experimental reports [41]. Xue et al. [42] showed that ratios between 0.30 and 0.50 wt% are appropriate for improving the performance of mixtures compared to specimens without capsules. Other experimental analyses [1,4] assessed the impact of different capsule ratios in asphalt mixtures (0.10, 0.25, and 0.50 wt%), showing that the percentage of broken capsules and the healing ratio between the specimens adopting the two highest amounts were similar. Figure 5 illustrates the numerical asphalt mixture for Case 2.

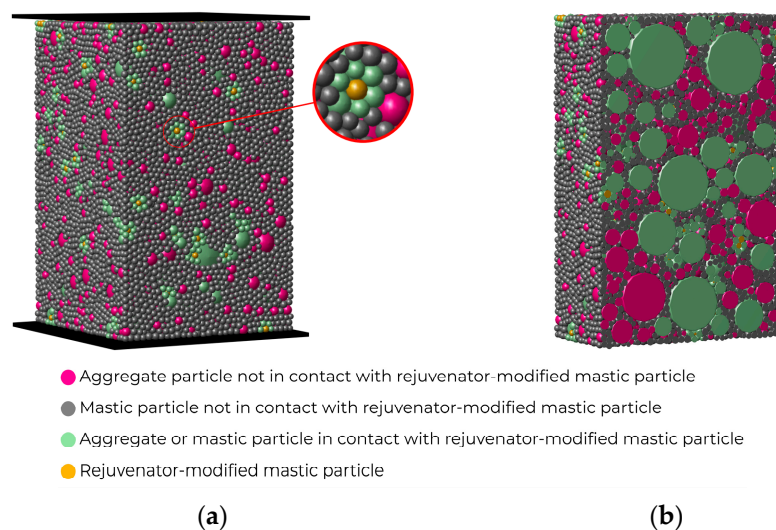


**Figure 5.** Asphalt mixture with a 0.30 wt% rejuvenator-modified mastic content, adopting a moderate influence effect (case 2): (a) numerical sample and (b) cross-section at mid-point.

Table 3 shows the predicted rejuvenator release rate corresponding to each rejuvenator-modified contact property, adopting a volume of influence with a diameter similar to the average capsule size. For instance, capsules should have a rejuvenator release rate of approximately 20.1% to generate the rejuvenator volume of 12.4% in the mastic and the respective influence on the stiffness properties of the asphalt mixture. Most authors considered higher release values [43,44], indicating that the rejuvenator modification effect can also be higher.

**Table 3.** Rejuvenator-modified particle properties.

Contact Property	Case 2			Case 3	
	$VR_{o/m}$ (%)	$V_{oil-influence}$ (mm <sup>3</sup> )	$R$ (%)	$V_{oil-influence}$ (mm <sup>3</sup> )	$R$ (%)
CM-2.5	1.7		2.8		12.7
CM-5	3.4		5.5		25.1
CM-10	6.6	2.54	10.7	11.49	48.5
CM-20	12.4		20.1		90.9

#### 4.3.3. Case 3

In Case 2, it was proposed that capsules affecting the mastic particles are in direct contact with them. However, the rejuvenator released from capsules can impact mastic particles that are not in direct contact with them. One crucial analysis to conduct is to attribute modifications to an enlarged volume to account for a broader rejuvenator influence. Accordingly, in Case 3, the rejuvenator effect in the mixture was extended to simulate, in an approximate way, the capillarity flow (when microcracks exist) and diffusion mechanisms. These mechanisms contribute to reducing the asphalt binder viscosity and easing its flow to close microcracks observed in experimental investigations [45,46].

In Case 3, it was admitted that the released rejuvenator homogeneously affected an extended volume centered in the original capsule location. The rejuvenator-modified particle dosage was 0.30 wt% (by weight of asphalt mixture), as in Case 2, and the volume of influence corresponded to a sphere with a diameter of 2.8 mm. The capsule modified all mastic particles, and their corresponding contacts, that were located within the adopted volume of influence.

This scenario represents the maximum influence that the presence of capsules may have on the stiffness properties of asphalt mixtures. In addition to the 2326 contacts directly adjusted by the modified elements mentioned in Case 2, an additional 16,202 interactions

also received appropriate rejuvenator-modified contact parameters. Figure 6 illustrates the numerical asphalt mixture with a 0.30 wt% capsule content (AM-30) for Case 3.

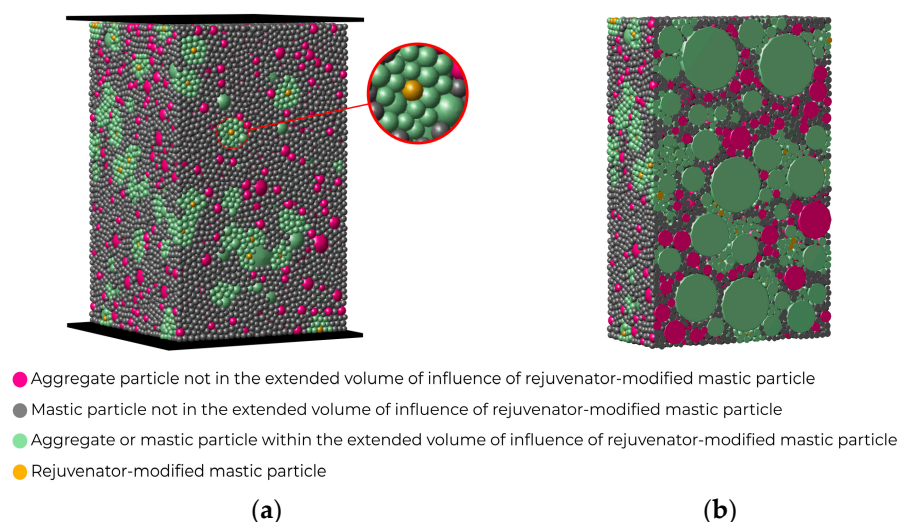


**Figure 6.** Asphalt mixture with a 0.30 wt% rejuvenator-modified mastic content adopting an extended influence effect (case 3): (a) numerical sample and (b) cross-section at mid-point.

Table 3 shows the predicted rejuvenator release rate corresponding to each rejuvenator-modified contact property, considering the extended volume of influence. Given this, capsules (size 1.7 mm) should have a rejuvenator release rate of nearly 91% to generate the rejuvenator volume of 12.4% in the mastic and the respective effect on the stiffness properties of the asphalt mixture. Experimental analyses to date suggest that calcium-alginate capsules, for example, can effectively release approximately 50% of their encapsulated rejuvenator volume under cyclic traffic loading conditions [43], limiting their coverage area to a certain level. Norambuena-Contreras et al. [8] also observed similar rejuvenator release ratios, confirming that rejuvenator content is a critical influential factor.

#### 4.4. Numerical Tests

The numerical asphalt mixture underwent uniaxial tension–compression cyclic tests with a strain-controlled amplitude of  $1.0 \times 10^{-4}$  m/m. Numerical simulations were carried out within the linear viscoelastic zone, and no damage was considered in the model. The simulations were performed at frequencies of 1, 2, 5, and 10 Hz, aligning closely with numerical simulations conducted in [36]. The applied strain is defined based on the upper-load plate position and specimen height, and the applied stress is defined considering the contact forces sum of the particles interacting with the upper plate and the cross-sectional area. The dynamic modulus and phase angle are calculated according to the following equations:

$$|E^*| = \frac{\sigma_{max} - \sigma_{min}}{\varepsilon_{max} - \varepsilon_{min}} \quad (17)$$

$$\phi = \frac{\Delta t}{T} \times 360 \quad (18)$$

where  $\sigma_{max}$  and  $\sigma_{min}$  are the maximum and minimum stress responses in a loading cycle,  $\varepsilon_{max}$  and  $\varepsilon_{min}$  are the maximum and minimum applied strain values in a loading cycle,  $\Delta t$  is the time lag between two adjacent peak stress and strain values, and  $T$  is the loading period.

## 5. Results and Discussion

For each of the three study cases, four different numerical analyses were carried out by assigning distinct contact properties to the rejuvenator-modified interactions based on various rejuvenator-to-bitumen ratios ranging from 2.5% to 20%. The numerical results

compare the responses obtained with specimens containing modified mastic particles to those obtained for the reference sample (without rejuvenator-modified elements).

It is worth noting that the numerical approach provides a reliable approximation of the capsule–asphalt mixture system by incorporating elements modified by the action of activated capsules directly into the particle model. The DEM model considers the random geometric distribution of these modified elements within the mixture, allowing for a more realistic representation.

### 5.1. Case Study 1

When considering all mastic particles modified by the rejuvenator, a noticeable reduction in the stiffness modulus was observed compared to the non-modified aggregate-to-mastic and mastic-to-mastic contacts in the reference sample (CM-0 only), as depicted in the numerical results presented in Figure 7a. The reduction in stiffness correlates with the rejuvenator-to-bitumen percentage, as indicated by the evolution of the stiffness modulus across the frequency range. In comparison with the control sample, the average reductions for specimens containing modified contacts, CM-2.5, CM-5, CM-10, and CM-20, were 42%, 57%, 79%, and 99%, respectively. Table 4 displays the variation in the stiffness modulus, revealing values ranging from 36.5% to 99.3% across the particle assemblies.

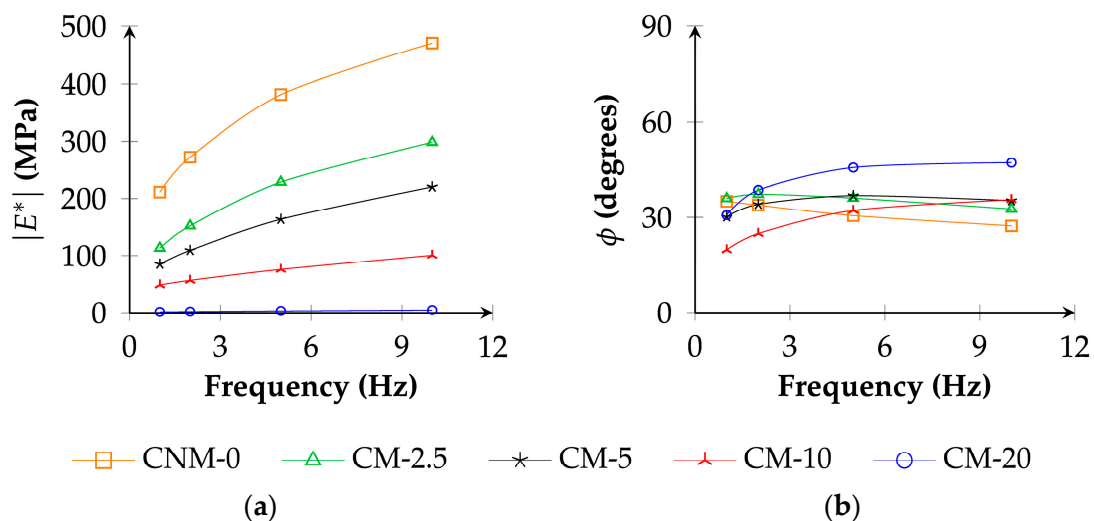


**Figure 7.** Numerical results for Case 1: (a) dynamic modulus and (b) phase angle.

**Table 4.** Rheological results for asphalt mixtures in Case 1.

Contact Property	Variation in Stiffness (%)		Difference in Phase Angle (°)	
	Min	(Max)	Min	(Max)
CM-2.5	36.5	(46.3)	0.92	(5.55)
CM-5	53.2	(59.8)	−4.93	(8.01)
CM-10	77.2	(80.2)	−15.26	(8.29)
CM-20	99.0	(99.3)	−4.34	(19.95)

Experimental reports considering a limited capsule content have suggested a maximum reduction of 30% [19,20,47]. The generated lower-stiffness mixture implies potential self-healing benefits for damaged asphalt pavement. However, the significant reduction, particularly for specimens with modified contact types, such as CM-10 and CM-20, adversely affected the mechanical behavior of the pavement structure due to the extended softened state of the asphalt layer, especially its deformation resistance, and it may eventually lead to structural problems [1].

Similar effects were observed for the phase angle (Figure 7b). In the virtual samples containing unmodified and CM-2.5-modified contacts, the phase angle changed as expected due to the impact of frequency (slightly decreases). For the asphalt mixture containing CM-2.5 contacts, the phase angle slightly increased by an average of 3.81° across the loading frequencies. This implies that the proportion of the elastic and viscous effects was not significantly different from that of the standard asphalt mixture. Still, the considerable reduction in the dynamic modulus may compromise essential mechanical parameters, requiring an acceptable (lower) amount of activated capsules.

Conversely, the phase angle performed differently than expected (decreased with frequency) for specimens that contained CM-5-, CM-10-, and CM-20-modified contacts, especially at frequencies lower than 5 Hz. This is a consequence of the significant degree of viscous state in the mastic. As indicated in Table 4, the deviation increased with the rise in rejuvenator content in the mastic, as reflected in the contact property type. The difference in the phase angle reached a maximum value of 19.95° for the specimen with the CM-20 contact property.

This case study showed that when all the mastic in an asphalt mixture is affected by the rejuvenator, there may be a significant change in rheological properties, with consequences for its performance.

### 5.2. Case Study 2

The numerical response for Case 2, which introduced a reasonable number of activated capsules into the mixture with a rejuvenator effect solely on particles in direct contact with them, is shown in Figure 8. As observed, the impact of the 0.30 wt% rejuvenator-modified mastic particles on the stiffness modulus and phase angle was subtle, regardless of the type of contact property (rejuvenator-to-bitumen amount). The average difference in the stiffness modulus of virtual asphalt mixtures with any modified contact type was around 0.4% compared to the control sample across the loading frequencies. A minimal variation was observed in specimens adopting the different contact property types. Table 5 illustrates that the range of stiffness modulus variation fell between 0.1% and 0.6%, indicating a limited influence on this property. Norambuena-Contreras et al. [5] reported a difference of less than 2% in the modulus of mixtures incorporating a slightly higher capsule ratio (0.50 wt% by weight of asphalt mixture), indicating that only a small amount of rejuvenator had been previously released into the asphalt mixture.

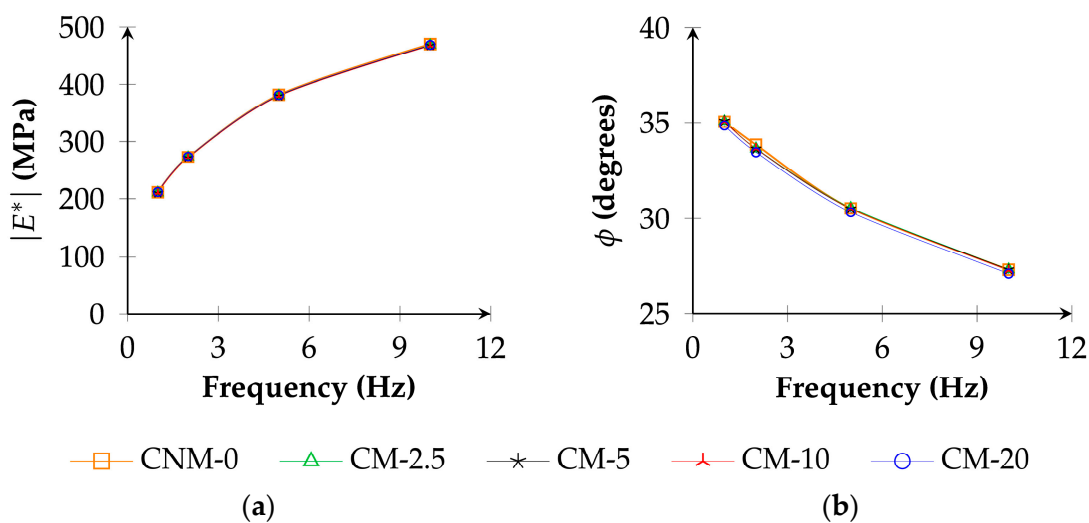


Figure 8. Numerical results for Case 2: (a) dynamic modulus and (b) phase angle.

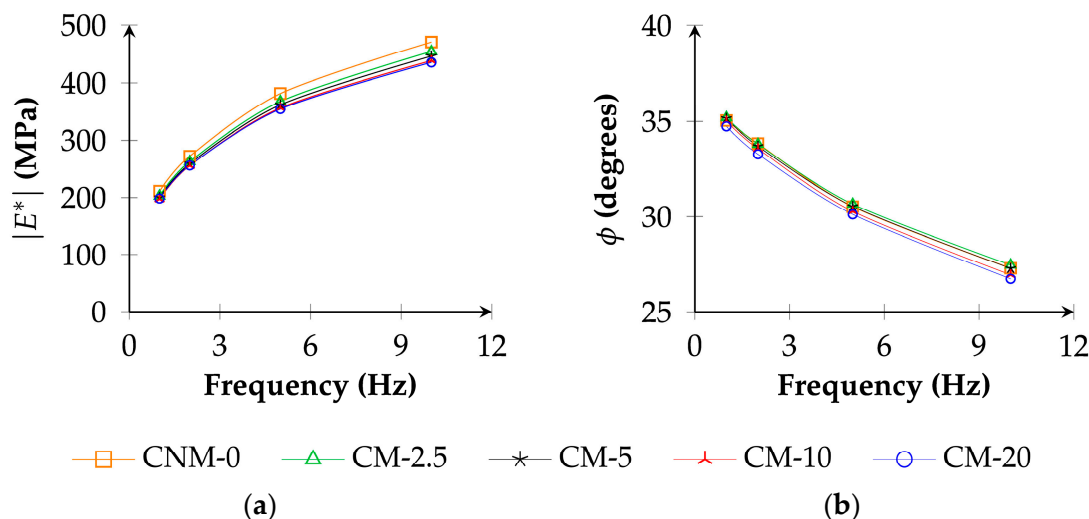
**Table 5.** Rheological results for asphalt mixtures in Case 2.

Contact Property	Variation in Stiffness (%)	Difference in Phase Angle (°)
	Min (Max)	Min (Max)
CM-2.5	0.1 (0.4)	−0.20 (0.02)
CM-5	0.2 (0.5)	−0.21 (0.04)
CM-10	0.3 (0.6)	−0.20 (0.01)
CM-20	0.2 (0.3)	−0.39 (−0.19)

Likewise, the difference in the phase angle, independently of the contact property adopted, was insignificant, ranging from  $-0.39^{\circ}$  to  $0.04^{\circ}$ , as shown in Table 5. This response indicates that a 0.30 wt% content did not affect the stiffness properties of asphalt mixtures. Additionally, the slight difference in the phase angle suggested that specimens with this number of modified elements generated adequate pavement performance under various loading conditions. It is important to point out that Case 2 considered a lower rejuvenator effect (small volume of influence with a diameter similar to the average capsule size) in the numerical sample, where only a few contacts (surrounding the 235 rejuvenator-modified elements) were affected.

### 5.3. Case Study 3

In the analysis of Case 3, an extended volume enveloping the rejuvenator-modified particles was adopted to simulate a robust capsule release and a widespread (diffusion) of the rejuvenator agent. Figure 9 illustrates the results corresponding to this scenario. The effect of the rejuvenator content was more pronounced in the stiffness properties of the numerical mixture compared to the previous case, especially for the stiffness modulus. In general, the stiffness modulus gradually reduced according to the adopted rejuvenator characteristics in the modified mastic particles, varying, on average, by 3.6%, 5.1%, 6.5%, and 6.7% for the modified contact properties CM-2.5, CM-5, CM-10, and CM-20, respectively.

**Figure 9.** Numerical results for Case 3: (a) dynamic modulus and (b) phase angle.

Similarly, a gradual increase in the minimum and maximum variations in the stiffness modulus was also observed with the increase in the rejuvenator effect (contact property). As shown in Table 6, the modulus variation ranged between 3.5% and 7.5% for specimens adopting the CM-2.5 and CM-20 contact properties, respectively.

**Table 6.** Rheological results for asphalt mixtures in Case 3.

Contact Property	Variation in Stiffness (%)	Difference in Phase Angle (°)
	Min (Max)	Min (Max)
CM-2.5	3.5 (3.9)	−0.03 (0.17)
CM-5	4.9 (5.3)	−0.14 (0.11)
CM-10	6.1 (6.9)	−0.34 (−0.04)
CM-20	6.0 (7.5)	−0.56 (−0.31)

The reduction in the stiffness modulus predicted with the proposed numerical framework was lower than the data available in experimental investigations in most cases. For example, Tabaković et al. [48] observed that compartmented alginate fibers with ratios of 0.23 wt% and 0.45 wt% reduced the stiffness modulus of asphalt mixtures by 10% to 20% (for the highest fiber amount). Additionally, Kargari et al. [20] reported a 10.8% reduction in the modulus of asphalt mixtures with a 0.35% capsule ratio. Al-Mansoori et al. [1] obtained a more significant reduction in the modulus (above 23%) with distinct capsule ratios (0.10, 0.25, and 0.50 wt%) in laboratory tests. A similar impact (around 20%) was also noted in the experimental work of García et al. [18].

Several aspects might contribute to the smaller effect observed in the numerical modeling results; for example, capsule and rejuvenator constitutive properties and rejuvenator release during the mixing and compaction processes [20]. In addition, García et al. [49] noticed that even capsules without incorporating any rejuvenator agent can affect the modulus of asphalt mixtures during laboratory analyses.

Similar to Case 2, the effect on the phase angle was equally low. The average difference in phase angle compared to the control sample was less than 0.78% across the loading frequencies, reaching differences that ranged from  $-0.56^\circ$  to  $0.17^\circ$ , as shown in Table 6. This result indicates that when a larger volume of influence was adopted, a slight decrease in both the stiffness modulus and the phase angle became evident for a capsule ratio of 0.30 wt%. This observation aligns with the study conducted by Norambuena-Contreras et al. [8], who suggested that capsule concentrations lower than 0.50 wt% do not significantly impact the rheological behavior of asphalt mixtures. Micaelo et al. [19] also reported similar results, where the capsule addition resulted in a difference of 11% in the dynamic modulus and only  $1.4^\circ$  in the phase angle.

Comparing the results with those obtained in Case 2, it is clear that the number of contacts affected by the modified mastic particles significantly highlighted the effect of the rejuvenator-to-bitumen contact properties on the rheological performance of asphalt mixtures. Nevertheless, both parameters impacted the stiffness properties of asphalt mixtures. In addition, the material stiffness reduction obtained for specimens containing CM-10- and CM-20-modified contacts was relatively similar. This result might indicate that capsules with release rates higher than 48.5% (see Table 3) produced a similar effect on the rheological behavior of asphalt mixtures for a 0.30 wt% capsule ratio, adjusting the rejuvenator amount whenever necessary.

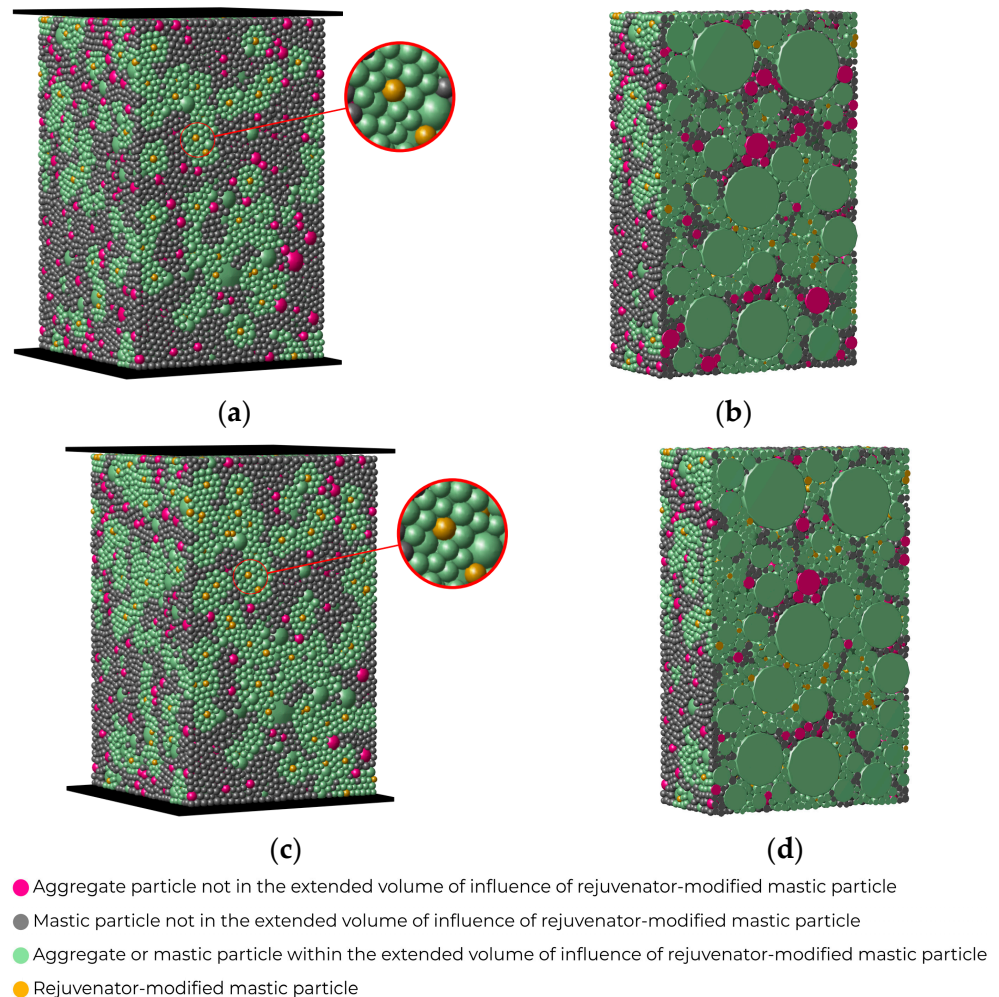
The particle model adopted in Case 3 (AM-30) is more representative of the expected rejuvenator effect on the rheological properties of mixtures than the particle model adopted in Case 2, which takes into account a lower rejuvenator effect (smaller volume of influence). The presented DEM simulations suggested that the rejuvenator-modified mastic content influences the asphalt mixture stiffness properties; however, the impact on the stiffness modulus was not as pronounced as some experimental analyses describe [18,47].

#### 5.4. Effect of Capsule Content (Case 3 Only)

Experimental studies have demonstrated that capsule ratios exceeding 0.50 wt% could lead to promising improvements in the mechanical behavior of asphalt mixtures [19]. Therefore, it is crucial to assess the impact of higher capsule ratios on the mechanical properties of asphalt pavements, as shown in the following case. For this purpose, two numerical as-

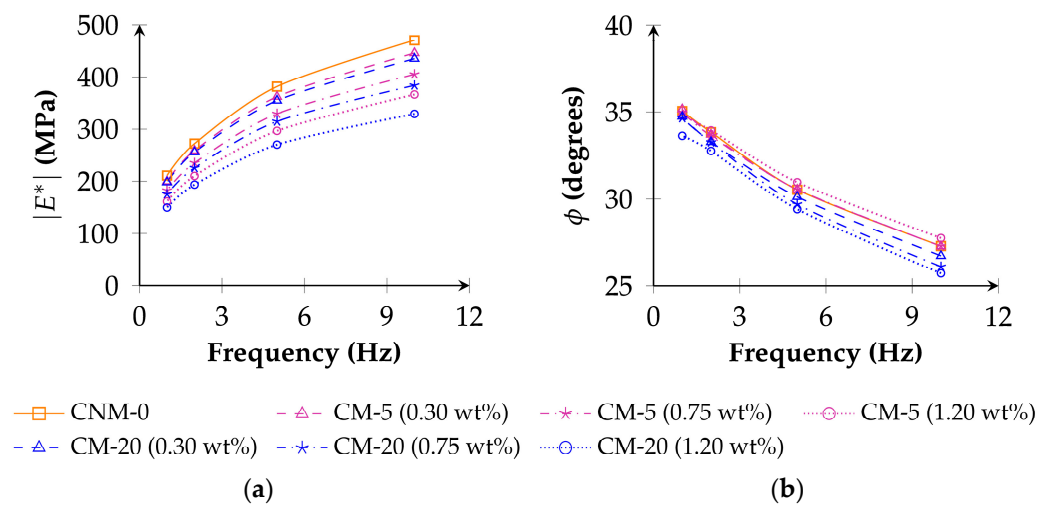
phalt mixtures, AM-75 and AM-120, incorporating 0.75 and 1.20 wt% rejuvenator-modified mastic ratios, corresponding to 588 and 940 randomly distributed particles within the mastic phase, respectively, were generated. These modified elements directly influenced the contact properties of 48,068 and 70,208 interactions in the particle assembly.

Figure 10 shows the virtual specimens and their internal cross-sections at the mid-point. Table 1 defines the contact properties (CM-5 and CM-20) adopted in this study, while Table 3 presents the rejuvenator release rate corresponding to each contact property (case 3). Uniaxial tension–compression cyclic loading tests were simulated, as in the previous analyses.



**Figure 10.** Asphalt mixture with rejuvenator-modified mastic, adopting an extended volume of influence and its internal cross-section at the mid-point: (a,b) AM-75, and (c,d) AM-120.

Figure 11 illustrates the rheological response for virtual mixtures AM-75 and AM-120 compared to the results obtained for the reference and AM-30 (Case 3). As can be seen, the increase of rejuvenator-modified mastic particles led to a more pronounced reduction in the stiffness modulus for both contact property cases (CM-5 and CM-20)—more contacts were adjusted in the assembly.



**Figure 11.** Numerical results for the reference sample and mixtures adopting modified contacts (CM-5 and CM-20) with capsule ratios of 0.30, 0.75, and 1.20 wt%: (a) dynamic modulus and (b) phase angle.

The presented numerical analysis also revealed that higher rejuvenator-to-mastic ratios resulted in a lower modulus (amplified rejuvenator effect on the mastic phase). This reduction was more apparent for virtual specimen AM-120, adopting the CM-20 property type, which agrees with laboratory studies that suggest capsules containing higher rejuvenator contents release more rejuvenator [8], thereby increasing the rejuvenator effect on the mixture modulus.

Table 7 indicates the variation in the stiffness modulus, showing a maximum reduction of 18.4% and 30% for assemblies AM-75 and AM-120, respectively. This reflects that the decrease was closely proportional to the number of activated capsules adopted in the particle model. The presented numerical modeling responses are consistent with the experimental results indicated in [19], where Micaelo et al. observed a decrease of 14% in the stiffness modulus for mixtures with a 1.00 wt% capsule content. Kargari et al. [20] also showed that the addition of 0.70% of capsules reduced the modulus of unaged asphalt mixtures by 15% in laboratory tests, which closely corresponds to the values obtained for specimen AM-75 for both scenarios of rejuvenator-modified mastic particles (CM-5 and CM-20).

**Table 7.** Rheological results for asphalt mixtures AM-30, AM-75, and AM-120.

Particle Assembly	Variation in Stiffness (%)		Difference in Phase Angle (°)	
	Min	(Max)	Min	(Max)
	CM-5	CM-20	CM-5	CM-20
AM-30	4.9	(5.3)	6.0	(7.2)
AM-75	13.5	(13.9)	17.0	(18.4)
AM-120	22.1	(23.6)	28.9	(30.0)

The variation in the phase angle with the addition of modified mastic particles was less pronounced. Table 7 shows that the deviation continuously extended with the addition of modified particle content, reaching a maximum value of 1.57° for AM-120, suggesting that an elevated number of modified mastic particles may negatively impact the rheological behavior of mixtures at some point.

The deviation in the phase angle response obtained for AM-75 and AM-120 in both rejuvenator-to-mastic scenarios was equivalent to those reported experimentally in [19] and to those obtained when adopting a capsule ratio of 0.30 wt% in the previous numerical modeling (Case 3). This suggests that the general rheological behavior of asphalt mixtures

remained unaffected at a high capsule amount of 1.20 wt% for the different rejuvenator-modified contact properties assigned.

The presented numerical simulations indicated that capsule contents between 0.30 and 0.75 wt% can be adopted without significantly compromising the rheological and mechanical properties of asphalt mixtures in the healed state. However, for higher capsule contents, the self-healing benefit may not be sufficient to outweigh the negative effects on the mechanical properties.

## 6. Summary and Conclusions

An innovative 3D DEM framework was employed to assess the non-homogeneous distributions of the rejuvenator, closely resembling real conditions in post-healed asphalt mixtures. The adopted 3D DEM meso-scale model incorporated the spatial distribution of rejuvenator-modified elements within the mixture specimens. It adopted a generalized Kelvin contact model to accurately represent the time-dependent behavior of asphalt materials. Uniaxial tension–compression numerical simulations were conducted to analyze different factors influencing the behavior of healed asphalt mixtures from a numerical point of view.

The ensuing discussion and case studies provided an initial contribution to understanding the behavior of post-healed asphalt mixtures. The main findings, crucial for future designs aiming at optimal post-healed behavior, are summarized as follows:

- When the entire particle assembly adopted rejuvenator-modified contacts, the asphalt mixture stiffness modulus reduced by between 37% and 99%. This decrease was attributed to a significant reduction in the binder viscosity, ultimately compromising the mechanical performance of the asphalt mixture. The phase angle performed differently than expected (decreased with frequency) in most analyses due to the excessively softened state.
- When a larger volume of influence was adopted (Case 3 vs. Case 2) to model the extended effect of encapsulated rejuvenators, a more noticeable impact on the stiffness modulus of mixtures was observed. For example, for cases considering a 0.30 wt% capsule content, the average reduction in the stiffness modulus verified in Case 2 and Case 3 reached 0.4% and 6.7%, respectively.
- For cases considering more suitable modified mastic ratios (less than 1.20 wt% of capsules content), the effect on the mixture stiffness modulus was, as expected, less pronounced. Numerical predictions indicated an average reduction in the modulus ranging from 3.6% to 29.3%. The phase angle was not significantly affected, aligning with known experimental reports that adopted a similar rejuvenator type and capsule content. These numerical findings suggested that the activated capsules within the studied contents did not have a meaningful impact on the rheological properties of asphalt mixtures.
- The rejuvenator-to-mastic ratio and the number of rejuvenator-modified contacts, associated with the mastic content and volume of influence, were influential parameters of the stiffness properties of asphalt mixtures.
- The effects on the asphalt mixture stiffness modulus observed in samples containing CM-10- and CM-20-modified contacts were relatively similar. This result suggested that capsules with release rates exceeding 48% produced a similar effect on the rheological properties of asphalt mixtures.
- The presented numerical simulations showed that the capsule content in asphalt mixtures can be increased up to 0.75 wt%, surpassing the often-used experimental test values of 0.50 wt%, without compromising their rheological properties. This increase may even have the potential to enhance their self-healing properties.

The presented numerical findings and future applications of the developed DEM framework will benefit the development of a more accurate capsule–asphalt mixture system to save maintenance costs, reduce maintenance operations, and extend the service life of asphalt pavements. It is important to note that the numerical results are based on a specific type of rejuvenator. Future studies will address rejuvenators with different properties, mixtures with different aggregate contents, and will aim to incorporate rejuvenator diffusion more realistically into the 3D DEM model, thereby better replicating the effect of encapsulated rejuvenators within the asphalt mixture.

**Author Contributions:** Conceptualization, N.M.A. and R.M.; methodology, G.C., N.M.A. and R.M.; software, G.C. and N.M.A.; validation, G.C.; investigation, G.C.; writing—original draft preparation, G.C.; writing—review and editing, N.M.A. and R.M.; visualization, G.C.; supervision, N.M.A. and R.M. All authors have read and agreed to the published version of the manuscript.

**Funding:** This work is part of the research activity of the third author carried out at Civil Engineering Research and Innovation for Sustainability (CERIS) and has been funded by Fundação para a Ciência e a Tecnologia (FCT) in the framework of project UIDB/04625/2020.

**Data Availability Statement:** Data are contained within the article.

**Conflicts of Interest:** The authors declare no potential conflict of interest concerning the research, authorship, and publication of this article.

## References

1. Al-Mansoori, T.; Micaelo, R.; Artamendi, I.; Norambuena-Contreras, J.; Garcia, A. Microcapsules for Self-Healing of Asphalt Mixture without Compromising Mechanical Performance. *Constr. Build. Mater.* **2017**, *155*, 1091–1100. [[CrossRef](#)]
2. Gómez-Meijide, B.; Ajam, H.; Garcia, A.; Vansteenkiste, S. Effect of Bitumen Properties in the Induction Healing Capacity of Asphalt Mixes. *Constr. Build. Mater.* **2018**, *190*, 131–139. [[CrossRef](#)]
3. Thejaswi, P.; Vengala, J.; Dharek, M.S.; Manjunatha, M.; Poudel, A. Sugarcane Bagasse Fibers for Enhancing Moisture Susceptibility Properties in Stone Mastic Asphalt. *Adv. Mater. Sci. Eng.* **2023**, *2023*, 5378738. [[CrossRef](#)]
4. Al-Mansoori, T.; Norambuena-Contreras, J.; Garcia, A. Effect of Capsule Addition and Healing Temperature on the Self-Healing Potential of Asphalt Mixtures. *Mater. Struct.* **2018**, *51*, 53. [[CrossRef](#)]
5. Norambuena-Contreras, J.; Yalcin, E.; Hudson-Griffiths, R.; Garcia, A. Mechanical and Self-Healing Properties of Stone Mastic Asphalt Containing Encapsulated Rejuvenators. *J. Mater. Civ. Eng.* **2019**, *31*, 04019052. [[CrossRef](#)]
6. He, Y.; Lv, S.; Wang, Z.; Ma, H.; Lei, W.; Pu, C.; Meng, H.; Xie, N.; Peng, X. Research on the Modulus Decay Model under a Three-Dimensional Stress State of Asphalt Mixture during Fatigue Damage. *Buildings* **2023**, *13*, 2570. [[CrossRef](#)]
7. García, Á.; Schlangen, E.; van de Ven, M.; Sierra-Beltrán, G. Preparation of Capsules Containing Rejuvenators for Their Use in Asphalt Concrete. *J. Hazard. Mater.* **2010**, *184*, 603–611. [[CrossRef](#)] [[PubMed](#)]
8. Norambuena-Contreras, J.; Liu, Q.; Zhang, L.; Wu, S.; Yalcin, E.; Garcia, A. Influence of Encapsulated Sunflower Oil on the Mechanical and Self-Healing Properties of Dense-Graded Asphalt Mixtures. *Mater. Struct.* **2019**, *52*, 78. [[CrossRef](#)]
9. Liu, Q.; Schlangen, E.; van de Ven, M. Induction Healing of Porous Asphalt Concrete Beams on an Elastic Foundation. *J. Mater. Civ. Eng.* **2013**, *25*, 880–885. [[CrossRef](#)]
10. Lou, B.; Sha, A.; Li, Y.; Wang, W.; Liu, Z.; Jiang, W.; Cui, X. Effect of Metallic-Waste Aggregates on Microwave Self-Healing Performances of Asphalt Mixtures. *Constr. Build. Mater.* **2020**, *246*, 118510. [[CrossRef](#)]
11. Ji, J.; Yao, H.; Suo, Z.; You, Z.; Li, H.; Xu, S.; Sun, L. Effectiveness of Vegetable Oils as Rejuvenators for Aged Asphalt Binders. *J. Mater. Civ. Eng.* **2017**, *29*, D4016003. [[CrossRef](#)]
12. Xu, S.; Liu, X.; Tabaković, A.; Schlangen, E. Experimental Investigation of the Performance of a Hybrid Self-Healing System in Porous Asphalt under Fatigue Loadings. *Materials* **2021**, *14*, 3415. [[CrossRef](#)]
13. Tabaković, A.; Faloon, C.; O’Prey, D. The Effect of Conductive Alginate Capsules Encapsulating Rejuvenator (HealRoad Capsules) on the Healing Properties of 10 Mm Stone Mastic Asphalt Mix. *Appl. Sci.* **2022**, *12*, 3648. [[CrossRef](#)]
14. Xu, S.; Liu, X.; Tabaković, A.; Schlangen, E. Investigation of the Potential Use of Calcium Alginate Capsules for Self-Healing in Porous Asphalt Concrete. *Materials* **2019**, *12*, 168. [[CrossRef](#)] [[PubMed](#)]
15. Suo, Z.; Nie, L.; Xiang, F.; Bao, X. The Effect of Waste Plant Oil on the Composition and Micro-Morphological Properties of Old Asphalt Composition. *Buildings* **2021**, *11*, 407. [[CrossRef](#)]
16. Quezada, J.C.; Chazallon, C. Complex Modulus Modeling of Asphalt Concrete Mixes Using the Non-Smooth Contact Dynamics Method. *Comput. Geotech.* **2020**, *117*, 103255. [[CrossRef](#)]
17. Micaelo, R.; Al-Mansoori, T.; Garcia, A. Study of the Mechanical Properties and Self-Healing Ability of Asphalt Mixture Containing Calcium-Alginate Capsules. *Constr. Build. Mater.* **2016**, *123*, 734–744. [[CrossRef](#)]
18. Garcia, A.; Austin, C.J.; Jelfs, J. Mechanical Properties of Asphalt Mixture Containing Sunflower Oil Capsules. *J. Clean. Prod.* **2016**, *118*, 124–132. [[CrossRef](#)]

19. Micaelo, R.; Freire, A.C.; Pereira, G. Asphalt Self-Healing with Encapsulated Rejuvenators: Effect of Calcium-Alginate Capsules on Stiffness, Fatigue and Rutting Properties. *Mater. Struct.* **2020**, *53*, 20. [[CrossRef](#)]
20. Kargari, A.; Arabani, M.; Mirabdolazimi, S.M. Effect of Palm Oil Capsules on the Self-Healing Properties of Aged and Unaged Asphalt Mixtures Gained by Resting Period and Microwave Heating. *Constr. Build. Mater.* **2022**, *316*, 125901. [[CrossRef](#)]
21. Concha, J.L.; Arteaga-Pérez, L.E.; Alpizar-Reyes, E.; Segura, C.; Gonzalez-Torre, I.; Kanellopoulos, A.; Norambuena-Contreras, J. Effect of Rejuvenating Oil Type on the Synthesis and Properties of Alginate-Based Polynuclear Capsules for Asphalt Self-Healing. *Road Mater. Pavement Des.* **2022**, *24*, 1669–1694. [[CrossRef](#)]
22. Xu, S.; Liu, X.; Tabaković, A.; Lin, P.; Zhang, Y.; Nahar, S.; Lommerts, B.J.; Schlangen, E. The Role of Rejuvenators in Embedded Damage Healing for Asphalt Pavement. *Mater. Des.* **2021**, *202*, 109564. [[CrossRef](#)]
23. Wang, F.; Zhang, L.; Yan, B.; Kong, D.; Li, Y.; Wu, S. Diffusion Mechanism of Rejuvenator and Its Effects on the Physical and Rheological Performance of Aged Asphalt Binder. *Materials* **2019**, *12*, 4130. [[CrossRef](#)] [[PubMed](#)]
24. Li, J.; Luo, C.; Jie, J.; Cui, H. Rheological Properties and Microscopic Morphology Evaluation of UHMWPE-Modified Corn Stover Oil Bio-Asphalt. *Buildings* **2023**, *13*, 2167. [[CrossRef](#)]
25. Norambuena-Contreras, J.; Concha, J.; Arteaga-Pérez, L.; Gonzalez-Torre, I. Synthesis and Characterisation of Alginate-Based Capsules Containing Waste Cooking Oil for Asphalt Self-Healing. *Appl. Sci.* **2022**, *12*, 2739. [[CrossRef](#)]
26. Cundall, P.A.; Strack, O.D. A Discrete Numerical Model for Granular Assemblies. *Geotechnique* **1979**, *29*, 47–65. [[CrossRef](#)]
27. Jin, C.; Li, S.; Yang, X.; Zhou, X.; You, Z. Aggregate Representation Approach in 3D Discrete-Element Modeling Supporting Adaptive Shape and Mass Property Fitting of Realistic Aggregates. *J. Eng. Mech.* **2020**, *146*, 04020042. [[CrossRef](#)]
28. Gao, L.; Zhang, Y.; Liu, Y.; Wang, Z.; Ji, X. Study on the Cracking Behavior of Asphalt Mixture by Discrete Element Modeling with Real Aggregate Morphology. *Constr. Build. Mater.* **2023**, *368*, 130406. [[CrossRef](#)]
29. Dan, H.-C.; Zhang, Z.; Chen, J.; Cao, W. Low-Temperature Fracture Characteristics of Asphalt Mixtures Using the Eccentric Single-Edge Notched Bend Test: A 3D Discrete Element Study. *Constr. Build. Mater.* **2022**, *344*, 128182. [[CrossRef](#)]
30. Abbas, A.; Masad, E.; Papagiannakis, T.; Harman, T. Micromechanical Modeling of the Viscoelastic Behavior of Asphalt Mixtures Using the Discrete-Element Method. *Int. J. Geomech.* **2007**, *7*, 131–139. [[CrossRef](#)]
31. Al Khateeb, L.; Anupam, K.; Erkens, S.; Scarpas, T. Micromechanical Simulation of Porous Asphalt Mixture Compaction Using Discrete Element Method (DEM). *Constr. Build. Mater.* **2021**, *301*, 124305. [[CrossRef](#)]
32. Liu, P.; Wang, C.; Lu, W.; Moharekpour, M.; Oeser, M.; Wang, D. Development of an FEM-DEM Model to Investigate Preliminary Compaction of Asphalt Pavements. *Buildings* **2022**, *12*, 932. [[CrossRef](#)]
33. Peng, Y.; Chen, Y.; Xu, Y.; Xia, S.; Lu, X.; Li, Y. Discrete Element Modelling of Mechanical Response of Crumb Rubber-Modified Asphalt Pavements under Traffic Loads. *Int. J. Pavement Eng.* **2022**, 1–18. [[CrossRef](#)]
34. Zhang, H.; Liu, H.; You, W. Microstructural Behavior of the Low-Temperature Cracking and Self-Healing of Asphalt Mixtures Based on the Discrete Element Method. *Mater. Struct.* **2022**, *55*, 18. [[CrossRef](#)]
35. Câmara, G.; Micaelo, R.; Monteiro Azevedo, N. 3D DEM Model Simulation of Asphalt Mastics with Sunflower Oil. *Comp. Part. Mech.* **2023**, *10*, 1569–1586. [[CrossRef](#)]
36. Câmara, G.; Azevedo, N.M.; Micaelo, R.; Silva, H. Generalised Kelvin Contact Models for DEM Modelling of Asphalt Mixtures. *Int. J. Pavement Eng.* **2023**, *24*, 2179625. [[CrossRef](#)]
37. Zhang, L.; Hoff, I.; Zhang, X.; Yang, C. Investigation of the Self-Healing and Rejuvenating Properties of Aged Asphalt Mixture Containing Multi-Cavity Ca-Alginate Capsules. *Constr. Build. Mater.* **2022**, *361*, 129685. [[CrossRef](#)]
38. Xu, S.; Tabaković, A.; Liu, X.; Schlangen, E. Calcium Alginate Capsules Encapsulating Rejuvenator as Healing System for Asphalt Mastic. *Constr. Build. Mater.* **2018**, *169*, 379–387. [[CrossRef](#)]
39. Al-Mansoori, T.; Norambuena-Contreras, J.; Micaelo, R.; Garcia, A. Self-Healing of Asphalt Mastic by the Action of Polymeric Capsules Containing Rejuvenators. *Constr. Build. Mater.* **2018**, *161*, 330–339. [[CrossRef](#)]
40. Bao, S.; Liu, Q.; Li, H.; Zhang, L.; Maria Barbieri, D. Investigation of the Release and Self-Healing Properties of Calcium Alginate Capsules in Asphalt Concrete under Cyclic Compression Loading. *J. Mater. Civ. Eng.* **2021**, *33*, 04020401. [[CrossRef](#)]
41. Li, R.; Zhou, T.; Pei, J. Design, Preparation and Properties of Microcapsules Containing Rejuvenator for Asphalt. *Constr. Build. Mater.* **2015**, *99*, 143–149. [[CrossRef](#)]
42. Xue, B.; Wang, H.; Pei, J.; Li, R.; Zhang, J.; Fan, Z. Study on Self-Healing Microcapsule Containing Rejuvenator for Asphalt. *Constr. Build. Mater.* **2017**, *135*, 641–649. [[CrossRef](#)]
43. Ruiz-Riancho, N.; Garcia, A.; Grossegger, D.; Saadoun, T.; Hudson-Griffiths, R. Properties of Ca-Alginate Capsules to Maximise Asphalt Self-Healing Properties. *Constr. Build. Mater.* **2021**, *284*, 122728. [[CrossRef](#)]
44. Zhang, L.; Liu, Q.; Li, H.; Norambuena-Contreras, J.; Wu, S.; Bao, S.; Shu, B. Synthesis and Characterization of Multi-Cavity Ca-Alginate Capsules Used for Self-Healing in Asphalt Mixtures. *Constr. Build. Mater.* **2019**, *211*, 298–307. [[CrossRef](#)]
45. Su, J.-F.; Schlangen, E.; Wang, Y.-Y. Investigation the Self-Healing Mechanism of Aged Bitumen Using Microcapsules Containing Rejuvenator. *Constr. Build. Mater.* **2015**, *85*, 49–56. [[CrossRef](#)]
46. Su, J.-F.; Zhang, X.-L.; Guo, Y.-D.; Wang, X.-F.; Li, F.-L.; Fang, Y.; Ding, Z.; Han, N.-X. Experimental Observation of the Vascular Self-Healing Hollow Fibers Containing Rejuvenator States in Bitumen. *Constr. Build. Mater.* **2019**, *201*, 715–727. [[CrossRef](#)]

47. Norambuena-Contreras, J.; Yalcin, E.; Garcia, A.; Al-Mansoori, T.; Yilmaz, M.; Hudson-Griffiths, R. Effect of Mixing and Ageing on the Mechanical and Self-Healing Properties of Asphalt Mixtures Containing Polymeric Capsules. *Constr. Build. Mater.* **2018**, *175*, 254–266. [[CrossRef](#)]
48. Tabaković, A.; Braak, D.; van Gerwen, M.; Copuroglu, O.; Post, W.; Garcia, S.J.; Schlangen, E. The Compartmented Alginate Fibres Optimisation for Bitumen Rejuvenator Encapsulation. *J. Traffic Transp. Eng.* **2017**, *4*, 347–359. [[CrossRef](#)]
49. García, Á.; Schlangen, E.; van de Ven, M. Properties of Capsules Containing Rejuvenators for Their Use in Asphalt Concrete. *Fuel* **2011**, *90*, 583–591. [[CrossRef](#)]

**Disclaimer/Publisher’s Note:** The statements, opinions and data contained in all publications are solely those of the individual author(s) and contributor(s) and not of MDPI and/or the editor(s). MDPI and/or the editor(s) disclaim responsibility for any injury to people or property resulting from any ideas, methods, instructions or products referred to in the content.